Synthetic developmental regulator MciZ targets FtsZ across species and inhibits bacterial division

Lidia Araújo-Bazán*[1], Sonia Huecas[1], Javier Valle [2], David Andreu[2], José M. Andreu*[1]

[1] Centro de Investigaciones Biológicas, CSIC, Madrid, Spain; [2] Department of Experimental and Health Sciences, Universitat Pompeu Fabra, Barcelona, Spain

*For correspondence. E-mail laraujo@cib.csic.es; j.m.andreu@cib.csic.es;

Tel +34 918373112; Fax +34 915360432

Summary. Cell division in most bacteria is directed by FtsZ, a conserved tubulin-like GTPase that assembles forming the cytokinetic Z-ring and constitutes a target for the discovery of new antibiotics. The developmental regulator MciZ, a 40-amino acid peptide that is endogenously produced during *Bacillus subtilis* sporulation, halts cytokinesis in the mother cell by inhibiting FtsZ. The crystal structure of a FtsZ:MciZ complex revealed that bound MciZ extends the C-terminal beta-sheet of FtsZ blocking its assembly interface. Here we demonstrate that exogenously added MciZ effectively inhibits *B. subtilis* cell division, sporulation and germination, and provide insight into MciZ molecular recognition by FtsZ from different bacteria. MciZ and FtsZ form a 1:1 complex with sub-micromolar affinity, analyzed by analytical ultracentrifugation, laser biolayer interferometry and isothermal titration calorimetry. Synthetic MciZ analogs, carrying single amino acid substitutions impairing MciZ beta-strand formation or hydrogen bonding to FtsZ, show a gradual reduction in affinity that resembles their impaired activity *in vivo*. Gene sequences encoding MciZ spread across genus *Bacillus* and synthetic MciZ slows down cell division in *Bacillus* species including pathogenic *B. cereus* and *B. anthracis.* Moreover, *B. subtilis* MciZ is recognized by the homologous FtsZ from *Staphylococcus aureus* and inhibits division when it is expressed into *S. aureus* cells.

Keywords: bacterial cytoskeleton, FtsZ inhibitors, *Bacillus*, *Staphylococcus aureus*

INTRODUCTION

Bacterial cell division is carried out by the concerted action of a macromolecular complex called the divisome (den Blaauwen *et al.*, 2017) and the cell wall synthesizing enzymes at the cytokinesis site (Egan *et al.*, 2017). Divisomal assembly is initiated in most bacteria by the formation of a ring-like scaffold of the cytoskeletal protein FtsZ at the nascent division site (Bi & Lutkenhaus, 1991). The Z-ring is attached to the inner side of the plasma membrane by FtsA and ZipA and recruits the rest of the division

machinery (Haeusser & Margolin, 2016; Xiao & Goley, 2016; Du & Lutkenhaus, 2017). The Z-ring precisely localizes to the mid cell by means of different regulatory factors that either induce FtsZ assembly at the division site or prevent FtsZ assembly at the poles or over unsegregated chromosomes (den Blaauwen *et al.*, 2017). In addition, metabolic sensors inhibit FtsZ assembly and control cytokinesis in response to the nutritional state of the cell (Weart *et al.*, 2007; Monahan & Harry, 2015). The Z-ring has a fast subunit turnover (Anderson *et al.*, 2004) and is composed of discrete FtsZ clusters that circumferentially treadmill guiding septal cell wall synthesis (Bisson-Filho *et al.*, 2017; Yang *et al.*, 2017; Monteiro *et al.*, 2018), leading to the scission of daughter cells. FtsZ is a tubulin-like GTPase whose subunits assemble head-to-tail forming polar filaments (Nogales *et al.*, 1998; Matsui *et al.*, 2012) that laterally associate into bundles trough the disordered C-terminal tails (Buske *et al*., 2015; Huecas *et al.*, 2017; Sundararajan *et al.*, 2018). GTP hydrolysis at the interface between monomers in filaments and a polymerization-driven structural switch enable FtsZ filament treadmilling dynamics (Artola *et al.*, 2017; Wagstaff *et al.*, 2017).

Due to its essential function in most bacteria, FtsZ is an attractive target (Lock & Harry, 2008), still clinically unexplored, for discovering new antibiotics that are urgently needed to counter the spread of resistant pathogens (World Health Organization, http://www.who.int/news-room/fact-sheets/detail/antibiotic-resistance). FtsZ inhibition blocks cell division, inducing the formation of larger undivided cells that subsequently die. Many experimental small molecule FtsZ inhibitors have been reported (den Blaauwen *et al.*, 2014; Schaffner-Barbero *et al.*, 2012), including GTP-replacing inhibitors (Ruiz-Avila *et al.*, 2013; Artola *et al.*, 2015) and allosteric modulators of the structural assembly switch (Elsen *et al.*, 2012; Artola *et al.*, 2017). The difluorobenzamide derivative PC190723 (Haydon *et al.*, 2008) and several of its analogs are currently the best characterized FtsZ-targeting antibacterials, including biochemical, structural, cellular and resistance mechanisms (Andreu *et al.*,

2010; Matsui *et al.*, 2012; Tan *et al.*, 2012; Stokes *et al.*, 2013; Kaul *et al.*, 2016; Adams *et al.*, 2016; Fujita *et al.*, 2017).

Starvation or harsh conditions induce *B. subtilis* cells to exit vegetative growth and binary fission and enter asymmetric sporulation, a form of reproduction that ensures storage and dissemination of the bacterial germline, until conditions permit spore germination and resuming growth. Expression of the transcription regulator Spo0A switches the Z-ring localization from midcell to the poles (Levin & Losick, 1996) via a spiral intermediate (Ben-Yehuda & Losick, 2002). Distinct programs of gene expression are initiated in the two cell types directed by sporulation-specific RNA polymerase σ factors, σ^F becoming active in the prespore and σ^E in the mother cell (Errington, 2003, Piggot & Hilbert, 2004). MciZ is a 40-amino acid developmental regulator that was discovered in a two-hybrid screen for FtsZ binding partners. MciZ is expressed during sporulation under the control of transcription factor σ^E, preventing Z-ring formation in the mother cell (Handler *et al.*, 2008). The crystal structure of a FtsZ:MciZ complex, formed by coexpressing His-tagged MciZ and a truncated version of *B. subtilis* FtsZ(12-315) including only the structured core of the protein, has revealed that MciZ binds at the C-terminal polymerization interface of FtsZ, the equivalent to the minus-end of tubulin, inhibiting FtsZ assembly by steric hindrance and shortening protofilaments (Bisson-Filho *et al.*, 2015). The cell division inhibitor SulA, which is expressed as part of the SOS system and stalls cell division in response to DNA damage, also binds the C-terminal polymerization interface (Cordell *et al.*, 2003).

We determined the cytological profile on *B. subtilis* cells of inhibitors targeting FtsZ on different binding sites, distinguishing them from antibiotics with other mechanisms of action, which should facilitate phenotypic screening. In addition to small molecules, a MciZ synthetic peptide was observed to inhibit *B. subtilis* cell division (Araujo-Bazan *et al.*, 2016). However, it was not known whether exogenous MciZ really targets intracellular FtsZ; and the possibility that MciZ could arrest cell division in other bacterial species had not been examined. Here we analyze the molecular recognition

of MciZ and peptide analogs with point changes by diverse FtsZ protein constructs, demonstrating FtsZ targeting in *B. subtilis* cells. In addition to cell division, excess MciZ inhibits sporulation and germination. MciZ homologs are encoded by other *Bacillus* species, and sensitivity to synthetic MciZ reaches pathogenic *B. cereus/anthracis*. We show that MciZ is also recognized by FtsZ from *S. aureus* and intracellular expression of MciZ inhibits *S. aureus* cell division.

RESULTS AND DISCUSSION

Exogenous MciZ effectively inhibits *Bacillus subtilis* cell division.

To characterize the action of synthetic MciZ on *B. subtilis*, we first quantified its effect on cell division, exposing cells to different concentrations of MciZ and determining the effect on cell length at different times (Fig. 1). The minimal concentration that inhibits *B. subtilis* cell division is 1 μM MciZ (Fig. 1A-B), according to our criterion to identify relevant inhibitors by induction of a strong filamentous phenotype (≥ three-fold increase in mean cell length (Araujo-Bazan *et al.*, 2016)). MciZ does not suppress initial growth under these conditions (mass doubling period, Fig. 1B), as expected for cell division inhibition (Arjes *et al.*, 2014). The minimum inhibitory concentration of growth (MIC_{90}) is 10 μM MciZ. We compared the time course of MciZ action with PC190723, a reference small molecule FtsZ inhibitor (Haydon *et al.*, 2008) (Fig. 1C). Both inhibitors had parallel filamenting effects: a relevant increase in cell length was observed following 80 min treatment with MciZ or PC190723. However, each of both inhibitors works by a different mechanism: MciZ blocks FtsZ polymer growth (Bisson-Filho *et al.*, 2015), whereas PC190723 binding stabilizes FtsZ polymers (Andreu *et al.*, 2010; Elsen *et al.*, 2012). MciZ increases the velocity of the directional treadmilling movement of NeonGreen-FtsZ around the division ring, whereas PC190723 halts FtsZ movement (Bisson-Filho *et al.*, 2017). Thus the available evidence indicated that exogenous MciZ is an effective inhibitor of *B. subtilis* cell division, which led us to an in depth study of the molecular mechanisms of MciZ action on bacterial cells.

Structure-based single amino acid changes in synthetic MciZ support FtsZ targeting in *B. subtilis* cells.

The crystal structure of the core FtsZ:MciZ complex shows that MciZ binds to the C-terminal subdomain of FtsZ, sterically interfering at the association interface with a next monomer to form FtsZ filaments (Bisson-Filho *et al.*, 2015). Bound MciZ folds into a α-helix (H1) preceded by a β-hairpin, formed by strands β1 and β2 that are disordered in free MciZ, and followed by a loop and a helical turn. Backbone hydrogen bonds between FtsZ strand β9 and MciZ strand β2 generate an extended β-sheet. There are hydrophobic interactions between helices H1 of MciZ and H10 of FtsZ, and between the β2/H1 loop of MciZ and the H10/β9 loop of FtsZ; a salt bridge between Arg20 of MciZ (H1) and Asp280 of FtsZ (H10) further stabilizes the complex (Fig. 2A-B).

We decided to challenge the MciZ:FtsZ recognition with synthetic point mutations in MciZ designed to disable these interactions (Fig. 2C), testing the effects of the modified synthetic peptides on living *B. subtilis* cells (Fig. 2D). We first eliminated the Arg20(MciZ)-Asp280(FtsZ) salt bridge, replacing Arg20 by Ala. However, peptide R20A was still active, showing effects similar to wild type MciZ (Fig. 2D). Replacing Arg20 for Asp (R20D) effectively disabled MciZ activity, so that no effect on cell length or FtsZ:GFP localization was observed (Fig. 2D). This result agrees with the reported lack of interaction (co-purification) of His_6-MciZ-R20D following co-expression with FtsZ (Bisson-Filho *et al.*, 2015). However, in our case the local charge inversion in R20D could also affect the exogenous MciZ peptide passage through the bacterial envelope prior to interacting with FtsZ in the cytosol; in addition R20D showed non-specific binding to purified FtsZ in our assays (see below). Therefore, we resorted to a more incisive strategy to inhibit MciZ:FtsZ interaction, namely disrupting β-sheet hydrogen bonding between β9 of FtsZ and β2 of MciZ, without any charge modification. We made different amino acid changes (Fig. 2C): i) replacing the conserved L12 with a β-sheet breaker residue (Leu12Pro) or with an unnatural D-amino acid (Leu12D-Leu), in order to disrupt the β2 strand in the middle and thus the β-sheet hydrogen bond

network; ii) specifically blocking backbone hydrogen bond formation between V10 of MciZ and S296 of FtsZ, or G14 of MciZ and M292 of FtsZ, by replacing these MciZ residues with the corresponding N-methyl-amino acids ($V10^{m}V$ and $G14^{m}G$). We found that MciZ activity was abrogated in each of the resulting analogs, except for $V10^{m}V$, which had a weak residual activity requiring higher concentration (40 μM) than the wild type (Fig. 2D). These results showed that single amino acid changes in MciZ, inspired by the crystal structure of the FtsZ:MciZ complex, impair its activity on cell division. They indicated that exogenous MciZ directly interacts with FtsZ in the treated *B. subtilis* cells, although these data did not discard other pathways.

The results of *in vitro* pull down assays of the different MciZ peptides with His_6-FtsZ recapitulated the cellular effects, supporting FtsZ targeting. FtsZ from *B. subtilis* (BsFtsZ) bound MciZ but not its L12P analog (Fig. 3A). A truncated version of BsFtsZ lacking the disordered C-terminal tail (His_6-BsFtsZ-ΔCt, residues 1-315) similarly recognized MciZ. These results are consistent with the lack of *in vivo* activity of L12P and confirmed that a single amino acid change is sufficient to disrupt the FtsZ:MciZ interaction; they also demonstrate that the C-terminal tail of BsFtsZ, which is not observed in crystal structures, is not necessary for the interaction with MciZ. The other MciZ analogs were also tested in pull down assays (Fig. 3B) and the results correlated with their *in vivo* activity. R20A and $V10^{m}V$, the only analogs that cause filamentation and modify FtsZ localization in cells (Fig. 2D), were retained by BsFtsZ similarly to MciZ. Thus, these amino acid changes do not abolish the recognition of MciZ by FtsZ. The peptide $G14^{m}G$ was weakly bound by FtsZ, consistent with its lack of activity on *B. subtilis*. No pull down signal was observed with L12l, similarly to L12P, indicating that disruption of the MciZ β2 strand blocks formation of the FtsZ:MciZ complex. A significant amount of R20D was retained by FtsZ despite its lack of effect on *B. subtilis* cells (Fig. 2D) and failure to co-purify with FtsZ (Bisson-Filho *et al.*, 2015). However, as it will be shown later this peptide interacts non-specifically with FtsZ, which may explain a false positive pull down result.

Following the reported ability of MciZ to inhibit FtsZ filament assembly by end capping (Bisson-Filho *et al.*, 2015), we confirmed that synthetic MciZ specifically reduces the light scattering increment and the amount of sedimenting polymer upon nucleotide-induced assembly of BsFtsZ under our conditions, in contrast with the inactive peptide L12P that does not affect BsFtsZ assembly (Fig. S1).

Molecular recognition of MciZ by FtsZ from different bacteria.

To gain insight into FtsZ:MciZ complex formation in solution, the interaction was monitored by co-sedimentation in analytical ultracentrifugation (AUC) experiments. Binding of MciZ to FtsZ was quantified by measuring the MciZ sedimentation velocity profiles in absence and presence of FtsZ (Fig. 4). BsFtsZ (Fig. 4A, B) and FtsZ from *Staphylococcus aureus* (SaFtsZ; Fig. 4C, D) both sedimented as monomers with $s_{20,w}$ = 3.0 S and 3.1 S respectively. The lighter MciZ and L12P free peptides sedimented at $s_{20,w}$ = 0.5 S - 0.6 S. However, in the presence of BsFtsZ or SaFtsZ practically no free MciZ signal was detected but the peptides co-sedimented with FtsZ, in a ratio of 0.9 peptide molecules per FtsZ molecule (Fig. 4E); most of the inactive L12P control sedimented as free peptide. These results demonstrated that MciZ specifically forms a 1:1 complex in solution with BsFtsZ and, importantly, they showed that *B. subtilis* MciZ is also recognized by the homolog SaFtsZ protein. We also analyzed BsFtsZ complex formation with the rest of MciZ analogs by co-sedimentation velocity (Fig. 4E and Fig. S2) and the results obtained were consistent with their *in vivo* activity, except $G14^{m}G$ that co-sedimented with FtsZ, which would be compatible with low-affinity binding.

We then characterized the kinetics of interaction between MciZ peptides and FtsZ proteins using bio-layer interferometry (BLI), which revealed different modes of interaction. In a first type of assay, a layer of His_6-BsFtsZ was immobilized on a biosensor tip using the His tag. This assay showed relatively rapid association of MciZ, R20A and $V10^{m}V$, with association rates around $8{\cdot}10^{4}$ $M^{-1}s^{-1}$ and slow dissociation rates around $8{\cdot}10^{-3}$ s^{-1}, giving high affinities with apparent $K_D \approx 0.1$ μM (Fig. 5), compatible

196 with a previous tryptophan fluorescence titration (Bisson-Filho *et al.*, 2015). No binding
197 was observed with the inactive peptide L12P. We then analyzed the interaction
198 between MciZ and different FtsZ species in reverse experiments using a His_6-MciZ
199 immobilized on the biosensor tip. The estimated binding affinities of BsFtsZ and
200 BsFtsZΔCt were similar (Fig. S3), confirming that the C-terminal region of BsFtsZ is not
201 necessary for the interaction with MciZ. Binding of SaFtsZ was about 5-fold weaker
202 than BsFtsZ in this BLI assay. The binding and dissociation kinetics were different from
203 the direct experiment and estimated K_D values were one order of magnitude higher,
204 possibly related to the different experimental configuration. The sensorgram with the
205 more distant Gram-negative FtsZ homolog from *Escherichia coli* (EcFtsZ) displayed
206 quite small changes that could not be fitted by a similar binding model.
207 Finally, the thermodynamic parameters of MciZ binding to FtsZ were determined by
208 isothermal titration calorimetry (ITC), a reference method to analyze biomolecular
209 interactions in solution (Freyer & Lewis, 2008). MciZ binding to FtsZ is endothermic (ΔH
210 = 3.3 kcal mol^{-1}), entropy driven ($-T\Delta S$ = -12.2 kcal mol^{-1}) (Fig. 6 and Table 1). This
211 thermodynamic profile is compatible with hydrophobic interactions in MciZ
212 polypeptide folding and binding to FtsZ. The equilibrium dissociation constant for the
213 interaction of MciZ with BsFtsZ is K_D = 0.26 ± 0.15 μM (Fig. 6A) and the close homolog
214 SaFtsZ has in fact 5-fold weaker affinity, K_D = 1.42 ± 0.60 μM (Fig. 6B). The inactive
215 peptide L12P showed a lack of ITC-detectable binding to BsFtsZ or SaFtsZ, supporting
216 specificity of the MciZ binding. The thermogram of the more distant Gram-negative
217 homolog EcFtsZ titrated with MciZ does not correspond to a binding isotherm, but
218 likely reflects non-specific interactions (Fig. 6C). The interactions of the other MciZ
219 analogs with BsFtsZ were also measured. The binding affinities of R20A and $V10^{m}V$ (K_D
220 values 0.16 ± 0.1 and 0.18 ± 0.08 μM respectively) are similar to MciZ. Binding of
221 $G14^{m}G$ is 7-fold weaker (K_D = 1.85 ± 0.62 μM) and the binding of L12⊥ is about 40-fold
222 weaker (Fig. S4 and Table 1). Peptide R20D was found to interact non-specifically with
223 FtsZ (Fig. S4B).

In summary, the results from the combined AUC, BLI and ITC approaches indicate the entropically driven formation of a 1:1 MciZ:BsFtsZ high-affinity complex (average K_D = 0.2 μM) in solution, whose features are consistent with the specific interactions described in the crystal structure of the core FtsZ:MciZ complex (Bisson-Filho *et al.*, 2015), particularly the β-sheet extension and hydrogen bonding pattern. The interaction was thus modulated or completely blocked by single amino acid substitutions in five synthetic MciZ variants. Their *in vivo* activities (Fig. 2) qualitatively correlate with their different *in vitro* binding affinities to BsFtsZ (Table 1), strongly supporting the notion that cellular FtsZ is being targeted by the exogenous MciZ peptide. Additionally, we have found that MciZ is specifically recognized by purified SaFtsZ and not by EcFtsZ, which points out the potential of MciZ to inhibit FtsZ and cell division in *S. aureus*, as will be described later.

Exogenously added MciZ or induced expression of *mciZ* block sporulation and germination in *B. subtilis*.

We next asked whether an excess of MciZ would interfere with the *B. subtilis* sporulation process. MciZ is normally expressed in the mother cell with a peak level 3.5 h after entry into sporulation, which contributes to block the formation of a Z-ring at mid-cell (Handler *et al.*, 2008). *B. subtilis* 168 cells, cultured first on a rich medium, were transferred to re-suspension medium to induce sporulation (Sterlini & Mandelstam, 1969). Microscopic analysis of the cultures 5 h later revealed the presence of spores in the samples growing without MciZ, but no spores and slightly filamented cells were observed in samples with 5 μM MciZ (Fig. 7A). These phenotypic changes are consistent with blocking FtsZ assembly both at mid-cell and at the prespore region, preventing the asymmetric cell division necessary for spore formation. As negative control, we repeated the experiment with the inactive peptide L12P and, as expected, the sporulation proceeded normally.

To ensure that the inhibitory effect of MciZ on sporulation was not due to potential membrane damage by the synthetic peptide, we examined sporulation in a *B. subtilis* strain harboring a xylose-inducible copy of *mciZ* (FG1443, Table S1). Control cells of FG1443 growing in re-suspension medium sporulated, but cells with 5 μM MciZ or 1% xylose did not form spores, demonstrating that exogenous MciZ or intracellular MciZ expression similarly block sporulation (Fig. 7A). Division of FG1443 cells was also inhibited by MciZ or xylose (Fig. S5).

We have also tested the effect of MciZ on the germination process. Germination is essential for dormant spores to return to vegetative growth, which is regulated by germination specific proteins synthesized during spore formation (Paredes-Sabja *et al.*, 2011). To induce germination, heat-activated spores were transferred to germination medium and the optical density of the cultures measured (Fig. 7B). Spores cultured in the absence of MciZ or with 5 μM L12P (inactive peptide) showed similar germination curves; however, exogenously added MciZ completely blocked germination in both strains. Intracellular expressed MciZ also impaired germination of the FG1443 strain. Our results demonstrate that MciZ can completely suppress *B. subtilis* reproduction since it is not only able to arrest vegetative growth by targeting FtsZ, but it can also prevent sporulation and germination, which are crucial for dissemination and survival.

Inhibition of cell division in different *Bacillus* species by synthetic *B. subtilis* and *B. anthracis* MciZ.

Conserved genomic sequences encoding homologs of the *B. subtilis* MciZ developmental regulator spread across *Bacillus* species, suggesting that MciZ confers a fitness advantage facilitating sporulation. However, MciZ is not essential for sporulation, probably due to redundancy with other factors preventing cytokinesis in the mother cell (Handler *et al.*, 2008). A phylogenetic tree constructed with the MciZ sequences ≥ 55 % identical to *B. subtilis* MciZ is shown in Fig. 8A. In addition to potential MciZs from *Bacillus spp*., a hypothetical 56-amino acid homolog with 46%

identity was found in *Clostridium ultunense* (GenBank: CCQ95631.1). Although there is substantial diversity between *Bacilli* and *Clostridia* sporulation processes (Paredes-Sabja *et al.*, 2014), in both cases the decision to enter sporulation falls on the transcriptional regulator Spo0A (Steiner *et al.*, 2011; Higgins & Dworkin, 2012) and on the activation cascade of sporulation-specific RNA polymerase sigma factors (Haraldsen & Sonenshein, 2003; de Hoon *et al.*, 2010); therefore, a functional MciZ would make sense in *Clostridium.* On the other hand, we recently noticed a 40-amino acid uncharacterized protein of *Streptococcus pneumoniae* (GenBank: CON26470.1) that is 100% identical to *B. subtilis* MciZ. However, given the lack of a confirmatory reference about MciZ presence in this species, and the absence of sporulation in *Streptococcus*, we could not explain this hypothetical MciZ coding sequence.

To explore the degree of specificity of MciZ action on different *Bacillus* species, we compared the inhibition of cell division by exogenous MciZ in two relatively distant *Bacillus* clades: the closely related group of *B. subtilis, B. amyloliquefaciens* and *B. licheniformis,* and the branch of the insecticidal *B. thuringiensis,* the food pathogen *B. cereus* and the anthrax agent *B. anthracis*, also very closely related among them (Fig. 8A). In order to permit comparisons in both directions, in addition to *B. subtilis* MciZ we synthesized MciZ from *B. anthracis* (Fig. 2C, $MciZ_{Bant}$). We cultured cells of the different *Bacillus spp*. in the presence of increasing non-toxic concentrations of each peptide and quantified their effects on division (Fig. 8B). *B. subtilis* was the more sensitive species: 2.5 μM MciZ or $MciZ_{Bant}$ led to a 6-7 fold increase in cell length. A higher concentration of MciZ (10 μM) was required for similar effects on the close *B. amyloliquefaciens* and *B. licheniformis*, which were less sensitive to $MciZ_{Bant}$ (40 μM). *B. thuringiensis-cereus-anthracis* were less sensitive than the *B. subtilis* group to MciZ and they showed no selectivity for $MciZ_{Bant}$, which lacked effect on *B. thuringiensis*. MciZ and $MciZ_{Bant}$ (40 μM) had small but significant effects on *B. anthracis* cell division (~2-fold increased cell length).

We concluded from these results that the specificity of MciZ action in *Bacillus* is low, which is compatible with the conservation of practically identical sequences in the MciZ binding zones of FtsZ in the six species examined. The different sensitivities to MciZ may thus be speculated to be related to differences in peptide permeability of their cell envelopes. On a practical side, the effects of MciZ on pathogenic *B. cereus*, *B. thuringiensis* and *B. anthracis* point to its potential use as antibacterial inhibitor. The infectious agent of anthrax is the dormant endospore and we have observed that MciZ or $MciZ_{Bant}$ added to the medium block sporulation on *B. cereus*, the closer relative of *B. anthracis*, although no effect on *B. cereus* germination was observed (Fig. S6).

Inhibition of *S. aureus* cell division by intracellular expression of *B. subtilis* MciZ.

The results obtained with AUC, BLI and ITC demonstrated that purified SaFtsZ recognizes MciZ from *B. subtilis*, consistent with small differences in the MciZ binding region of FtsZ between BsFtsZ and SaFtsZ (Fig. 9A). However, we observed that *S. aureus* Mu50 is not sensitive to exogenously provided MciZ. Taking into account differences in cell wall composition and architecture among gram positive bacteria (Kim *et al.*, 2015) and insights into the interaction of antimicrobial peptides with those cell wall components (Malanovic & Lohner, 2016), we thought that exogenous MciZ was ineffective on *S. aureu*s, possibly because it cannot enter the cell. To test this hypothesis we generated a *S. aureus* strain harboring a plasmid with an inducible copy of *mciZ* (strain RN4220 + pCN51-P_{cad}-*mciZ*, Table S1). When we grew this strain in the presence of cadmium to induce *mciZ* expression we observed enlarged "ballooning" cells, a phenotype characteristic of blocking cell division in cocci (Haydon *et al.*, 2008; Pinho & Errington, 2003). Additionally, using a fluorescent probe that we had developed to label FtsZ polymers (Artola *et al.*, 2017), we could confirm the absence of Z-rings in these enlarged cells (Fig. 9B). The treated cells had a mean diameter 1.55-fold larger than the control cells (Fig. 9C). In the case of *E. coli*, we did not observe any effects on cell division with exogenously added or endogenously inducible MciZ (strain

BL21+pAB50, Table S1), which is consistent with the lack of specific binding of MciZ to EcFtsZ that had been observed *in vitro.* These results may be explained by the weak conservation of the MciZ binding residues in EcFtsZ (Fig. 9A). Our results also suggest the possibility of developing MciZ-based peptide antibacterials against *S. aureus*. One possibility would be the use of vectors such as cell-penetrating peptides (Copolovici *et al.*, 2014), an approach that has been broadly explored for drug delivery to tumor cells (Wang & Wang, 2012) and less often against infectious diseases (de la Torre *et al.*, 2014). As a preliminary test, we tried synthetic MciZ fused to a N-terminal cell-penetrating Tat sequence that enhanced filamentation and toxicity on *B. subtilis*, but lacked effect on *S. aureus* (40 μM Tat-MciZ); additional possibilities remain to be studied.

Conclusion.

We have shown that exogenous MciZ peptides inhibit *B. subtilis* cell division, sporulation and germination, and have analyzed in detail MciZ molecular recognition by different FtsZ. The cell division inhibitory activity of synthetic MciZ extends to pathogenic *B. cereus* - *B. anthracis.* Given the complexity of the sporulation process, where many factors are involved, we cannot discard the possibility that another cellular mechanism or receptor, in addition to direct inhibition of FtsZ assembly, might explain the selective action of MciZ in *Bacillus*. However, based on the results obtained with *S. aureus*, a non-spore forming pathogen, we propose that entry or expression of *B. subtilis* MciZ within bacterial cells is sufficient to inhibit division as long as the MciZ recognition elements helix H10-strand β9 of FtsZ are conserved. Our results suggest the possibility of developing MciZ-based peptide antibacterial agents targeting cell division.

EXPERIMENTAL PROCEDURES

Peptides. MciZ and the analogs shown in Fig. 2C were assembled on either Prelude (Gyros Protein Technologies, Tucson, AZ) or microwave-assisted Liberty Blue (CEM Corp., Matthews, NC) synthesizers, using ChemMatrix (PCAS Biomatrix Inc., Saint-Jean-sur-Richelieu, Quebec, Canada) or 2-chlorotrityl chloride (Iris Biotech GmbH, Marktredwicz, Germany) resins, respectively, and optimized Fmoc solid phase synthesis protocols, including the N-methyl substituted Fmoc-MeVal and Fmoc-N-MeGly residues in V10^{m}V and G14^{m}G, respectively. For coupling onto MeVal and MeGly residues the synthesis was switched to manual mode, the respective peptide resins were first deprotected with piperidine/dimethylformamide (DMF) (20% v/v, 2 x 10 min) and piperidine/1,8-diazabicyclo(5.4.0)undec-7-ene/toluene/DMF (5 : 5 : 20 : 70, v/v; 2 x 5 min), then the incoming Fmoc-Gly^{9} and Fmoc-Val^{13} were respectively added to the resin in 5-fold molar excess, along with 7-azabenzotriazol-1-yloxy)tripyrrolidinophosphonium hexafluorophosphate (PyAOP) and N,N-diisopropylethylamine (5- and 10-fold molar excess, respectively), in DMF as solvent and allowed to react for 1 h with intermittent manual stirring. An additional (2.5 molar excess) amount of PyAOP was next added and the mixture stirred for another 60 min. Synthesis was then resumed in automated mode for the remaining residues of each sequence.

After deprotection and cleavage with trifluoroacetic acid/H_2O/triisopropylsilane (95:2.5:2.5 v/v, 90 min, r.t.), the peptides were isolated by precipitation with cold ethyl ether, reconstituted in water and lyophilized. Preparative reverse phase HPLC purification yielded the target peptides in >95% homogeneity, with mass spectra consistent with the expected composition. Additional peptides (not listed on Fig. 2C) included versions of both MciZ and R20A elongated at the N-terminus with the Tat(48-60) (GRKKRRQRRRPPQ) cell-penetrating sequence.

Peptide stock solutions (5 mM) were prepared in distilled water before use. Concentration was measured spectrophotometrically using an extinction coefficient of

13980 $M^{-1}cm^{-1}$ at 280 nm, calculated from the amino acid sequence. PC190723 was synthesized as previously described (Andreu *et al.*, 2010) and stock solutions prepared in dimethyl sulfoxide, whose residual concentration in treated cultures and controls was less than 0.5%.

Bacterial strains, plasmids and microscopy. All strains and plasmids used in this work are listed in Table S1. *Bacillus spp*, except *B. anthracis*, were grown in cation adjusted Mueller-Hinton broth (CAMHB; Becton, Dickinson and Company) at 37ºC. *B. anthracis* was grown in Nutrient Broth medium (beef extract 5 g/L, peptone 10 g/L, NaCl 5 g/L, pH 7.2) and manipulated at the Neglected and Emerging Diseases Unit of the VISAVET Health Surveillance Centre (Universidad Complutense de Madrid, Spain). *S. aureus* RN4220 was grown in Trypticasein Soy Broth (TSB, Eur Pharm, Pronadisa) at 37ºC. MIC values were determined by a broth macrodilution method as described (Artola *et al.*, 2015).

To construct plasmid pCN51-P_{cad}-*mciZ,* a 124 bp fragment containing the *mciZ* open reading frame was amplified using primers mciZ-BamHI (5'-AAGGATCCATGAAAGTGCACCGCAT-3') and mciZ-EcoRI (5'-AAGAATTCTTATGGCTTTGAGATCCAATC-3'). The PCR product was digested with BamHI and EcoRI (sites underlined in primer sequences above) and cloned into pCN51, cut with the same enzymes. Expression of *mciZ* was induced by 2.5 μM $CdCl_2$. Antibiotics were used at the following concentrations: chloramphenicol, 5 μg/mL; spectinomycin, 100 μg/mL; erythromycin, 10 μg/mL; kanamycin, 50 μg/mL; ampicillin, 100 μg/mL. Microscopy assays were performed as previously described (Araujo-Bazan *et al.*, 2016). *B. anthracis* was previously subjected to Gram staining.

Sporulation and germination assays. *B. subtilis* or *B. cereus* cells were grown in CAMBH at 37ºC, inoculated at an OD_{600} of 0.05 from an overnight culture grown in the same medium. When the culture reached OD_{600} 0.14, sporulation was induced by transferring cells to the re-suspension medium of Sterlini and Mandelstam (Sterlini & Mandelstam, 1969). After 24 hours in sporulation medium spores were harvested

418 (3,000 g, 15 min, 4°C) and resuspended in 50 mM potassium phosphate buffer (pH 8.0)
419 with phenylmethylsulfonyl fluoride (1 mM), lysozyme (10 mg/mL), DNase-I (25 μg/mL)
420 and RNase (25 μg/mL) and samples were incubated 60 min at 30°C to eliminate
421 possible vegetative cells (Seydlova & Svobodova, 2012). The intact spores were
422 sedimented by centrifugation (3,000 g, 10 min, 4°C), washed three times with distilled
423 water and stored at 4°C. All spores used for germination were first heat-activated in
424 distilled water for 30 min at 70°C. Germination of heat-activated spores was triggered
425 in CAMHB medium supplemented with 10 mM L-asparagine, 10 mM glucose, 1 mM
426 fructose, and 1 mM potassium chloride (Pandey *et al.*, 2013).

427 **Protein purification.** BsFtsZ, BsFtsZΔCt (Huecas *et al.*, 2017), SaFtsZ and EcFtsZ
428 (Artola *et al.*, 2017) were purified as described. His_6-BsFtsZ and His_6-BsFtsZΔCt were
429 purified as BsFtsZ and BsFtsZΔCt, respectively, but without the His-tag cleavage step.
430 BsFtsZ polymerization was monitored by light scattering and sedimentation in 50 mM
431 Hepes-KOH, 300 mM KCl, 1 mM EDTA, 10 mM $MgCl_2$, 100 μM GMPCPP, pH 6.8 at 25 °C
432 as described (Ruiz-Avila *et al.*, 2013).

433 His_6-MicZ for BLI assays was expressed in *E. coli* BL21 cells transformed with plasmid
434 pAB50. The expression was induced with 1 mM isopropyl-β-D-thiogalactopyranoside.
435 After 3 h of induction at 37 °C, cells were harvested by centrifugation and the pellet
436 was resuspended in 50 mM Hepes-KOH, 300 mM KCl, 1 mM EDTA, pH 6.8,
437 supplemented with 0.1 mM GDP. Cells were lysed by sonication, the lysate was cleared
438 by centrifugation at 20,000 g for 20 min at 4°C, and directly applied to the biosensor.

439 **Pull down assay.** For *in vitro* MciZ binding assays, 30 μM purified His_6-BsFtsZ or His_6-
440 BsFtsZΔCt was incubated with 25 μL of nickel NTA agarose beads (ABT) for 1 h at 4°C,
441 in binding buffer (50 mM NaH_2PO_4, 300 mM NaCl, 10 mM imidazole, pH 8.0). The
442 beads were washed three times at 500 g with washing buffer (50 mM NaH_2PO_4, 300
443 mM NaCl, 20 mM imidazole, pH 8.0) and washed beads, with His_6-BsFtsZ or His_6-
444 BsFtsZΔCt bound, were incubated with 30 μM MciZ or analogs in binding buffer for 1 h
445 at 4°C. The beads were then washed three times and bound proteins were eluted with

446 elution buffer (50 mM NaH_2PO_4, 300 mM NaCl, 250 mM imidazole, pH 8.0). Eluted
447 proteins were separated by SDS-PAGE and stained using Coomassie blue.

448 **Analytical ultracentrifugation (AUC).** Sedimentation velocity experiments were
449 made in a Beckman Optima XL-I analytical ultracentrifuge equipped with interference
450 and absorbance optics, using an An50/Ti rotor with 12-mm double-sector centerpieces
451 at 45,000 rpm, 25 °C. Differential sedimentation coefficient distributions, c(s), were
452 calculated with SEDFIT (Schuck *et al.*, 2002). The weight average sedimentation
453 coefficient values measured in buffer at 25 °C were corrected to H_2O at 20°C, $s_{20,w}$. The
454 protein concentration was measured by refractive index increment (to which the lower
455 mass peptide contributes very little) and the peptide was measured by absorption at
456 295 nm (subtracting the contribution of the proteins, which lack Trp residues and
457 absorb less than MciZ at this wavelength). The area under the peak in the c(S)
458 distribution of the peptide and initial scans at 3,000 rpm were employed to calculate
459 the fraction of peptide co-sedimenting with the protein (Barbier *et al.*, 2010). AUC
460 experiments were done in 50 mM Hepes-KOH, 300 mM KCl, 1 mM EDTA, pH 6.8,
461 supplemented with 0.1 mM GDP.

462 **Bio-layer interferometry (BLI)**. The interaction between peptides and BsFtsZ was
463 analyzed using a single channel BLItz system with Ni-NTA biosensors (ForteBio, Menlo
464 Park, CA, USA). His_6-BsFtsZ was immobilized through the His-tag on the sensors, at a
465 final concentration of 100 μg/mL in 50 mM Hepes-KOH, 300 mM KCl, 1 mM EDTA, pH
466 6.8, supplemented with 0.1 mM GDP. Experiments were performed at ~22 °C and a
467 shake speed of 2,200 rpm, with baseline for 30 s followed by an association phase
468 (experimental sample) for 180 s and a dissociation phase (buffer alone) for 180 s. The
469 interacting peptides in the same buffer were added to generate the sensorgrams. The
470 best fit association and dissociation rate constants were determined using the BLItz
471 Pro software and Sigma Plot (Systat Software). The interaction between MciZ and
472 different species of FtsZ was analyzed in reverse experiments in which His_6-MciZ was

immobilized on the biosensor tip. The interacting proteins (BsFtsZ, BsFtsZΔCt, SaFtsZ or EcFtsZ, 100 μg/ml) were added in the same buffer.

Isothermal titration calorimetry (ITC). ITC measurements were performed using a MicroCal PEAQ-ITC calorimeter (Malvern). The sample cell (0.2 mL) was loaded with 10 μM FtsZ, equilibrated in the experimental buffer with a Fast Desalting Column HR 10/10 (Pharmacia Biotech), and the syringe was loaded with the peptide at a concentration comprised between 200 and 250 μM. Experiments were performed in 50 mM Hepes-KOH, 300 mM KCl, 1 mM EDTA, pH 6.8, supplemented with 0.1 mM GDP. Concentrated stock solutions of peptide in water were diluted to the experimental concentrations in buffer. An identical small proportion of water was introduced in the protein sample. As a control experiment, the individual dilution heats for the syringe reactant were determined by carrying out identical injections of the reactant into the sample cell with buffer. Controls without peptide and buffer in buffer controls were also run. A total of 13 injections of 3 μL were sequentially mixed into the sample cell with 180 s spacing. The electrical power required to maintain the reaction cell at constant temperature after each injection was recorded as a function of time, generating the thermograms shown. Binding isotherms were fitted to a single type of site model using the MicroCal PEAQ-ITC Analysis software.

Phylogenetic tree. Phylogenic analysis was performed on the Phylogeny.fr platform (http://www.phylogeny.fr/) (Dereeper *et al.*, 2008). Sequences were aligned with MUSCLE (v3.8.31) configured for highest accuracy. The phylogenetic tree was reconstructed using the maximum likelihood method implemented in the PhyML program (v3.1/3.0 aLRT). The WAG substitution model was selected assuming an estimated proportion of invariant sites (of 0.084) and 4 gamma-distributed rate categories to account for rate heterogeneity across sites. The gamma shape parameter was estimated directly from the data (gamma=2.455). Reliability for internal branch was assessed using the aLRT test (SH-Like). Graphical representation and edition of the phylogenetic tree were performed with TreeDyn (v198.3).

ASSOCIATED CONTENT

Supporting Information available: Table S1, Figures S1-S6

ACKNOWLEDGEMENTS

We thank Dr. M. A. Jimenez, Institute of Physical Chemistry Rocasolano (IQFR), CSIC Madrid, for valuable help designing MciZ peptide analogs and discussions; Dr. M. Menéndez, IQFR, CSIC Madrid, for advice on ITC and discussions; Drs. M.A. Peñalva and M. Espinosa, Centro de Investigaciones Biológicas, for critical reading of the manuscript. We especially thank Dr. Nerea García and Irene Martínez, Neglected and Emerging Diseases Unit of the VISAVET Health Surveillance Centre (Universidad Complutense de Madrid, Spain), for *B. anthracis* growth and manipulation. We thank Dr. F. Gueiros-Filho, University of Sao Paulo, Brasil; Dr. A. Bisson-Filho, Harvard University, USA; Dr. E. Harry, ithree institute, University of Technology, Australia; and Dr. I. Lasa, Universidad Pública de Navarra, Spain, for kindly providing strains and plasmids. We thank David Juan, Centro de Investigaciones Biológicas (CIB), CSIC, Madrid, for FtsZ protein purification, and the Medicinal Chemistry laboratory (Dr. M. L. López-Rodríguez), Universidad Complutense de Madrid, Spain, for synthesizing PC190723.This work was funded by MINECO grants BFU 2014-51823-R to JMA and AGL2014-52395-C2 to DA.

AUTHOR CONTRIBUTIONS

L.A-B., D.A. and J.M.A. designed experiments, L.A-B. performed the experiments, S.H. performed the ITC experiments, J.V. synthesized the peptides, L.A-B and J.M.A. wrote the manuscript with input from the other authors.

REFERENCES

Adams, D.W., L.J. Wu & J. Errington. (2016) A benzamide-dependent ftsZ mutant reveals residues crucial for Z-ring assembly. *Mol Microbiol* **99**: 1028-1042. DOI: 10.1111/mmi.13286.

Anderson, D.E., F.J. Gueiros-Filho & H.P. Erickson. (2004) Assembly dynamics of FtsZ rings in Bacillus subtilis and Escherichia coli and effects of FtsZ-regulating proteins. *J Bacteriol* **186**: 5775-5781. DOI: 10.1128/JB.186.17.5775-5781.2004.

Andreu, J.M., C. Schaffner-Barbero, S. Huecas, D. Alonso, M.L. Lopez-Rodriguez, L.B. Ruiz-Avila*, et al.* (2010) The antibacterial cell division inhibitor PC190723 is an FtsZ polymer-stabilizing agent that induces filament assembly and condensation. *J Biol Chem* **285**: 14239-14246. DOI: 10.1074/jbc.M109.094722.

Araujo-Bazan, L., L.B. Ruiz-Avila, D. Andreu, S. Huecas & J.M. Andreu. (2016) Cytological Profile of Antibacterial FtsZ Inhibitors and Synthetic Peptide MciZ. *Front Microbiol* **7**: 1558. DOI: 10.3389/fmicb.2016.01558.

Arjes, H.A., A. Kriel, N.A. Sorto, J.T. Shaw, J.D. Wang & P.A. Levin. (2014) Failsafe mechanisms couple division and DNA replication in bacteria. *Curr Biol* **24**: 2149-2155. DOI: 10.1016/j.cub.2014.07.055.

Artola, M., L.B. Ruiz-Avila, E. Ramirez-Aportela, R.F. Martinez, L. Araujo-Bazan, H. Vazquez-Villa*, et al.* (2017) The structural assembly switch of cell division protein FtsZ probed with fluorescent allosteric inhibitors. *Chemical Science* **8**: 1525-1534. DOI: 10.1039/C6SC03792E.

Artola, M., L.B. Ruiz-Avila, A. Vergonos, S. Huecas, L. Araujo-Bazan, M. Martin-Fontecha*, et al.* (2015) Effective GTP-replacing FtsZ inhibitors and antibacterial mechanism of action. *ACS Chem Biol* **10**: 834-843. DOI: 10.1021/cb500974d.

Barbier, P., A. Dorleans, F. Devred, L. Sanz, D. Allegro, C. Alfonso*, et al.* (2010) Stathmin and interfacial microtubule inhibitors recognize a naturally curved conformation of tubulin dimers. *J Biol Chem* **285**: 31672-31681. DOI: 10.1074/jbc.M110.141929.

Ben-Yehuda, S. & R. Losick. (2002) Asymmetric cell division in B. subtilis involves a spiral-like intermediate of the cytokinetic protein FtsZ. *Cell* **109**: 257-266. DOI: 10.1016/S0092-8674(02)00698-0.

Bi, E.F. & J. Lutkenhaus. (1991) FtsZ ring structure associated with division in Escherichia coli. *Nature* **354**: 161-164. DOI: 10.1038/354161a0.

Bisson-Filho, A.W., K.F. Discola, P. Castellen, V. Blasios, A. Martins, M.L. Sforca*, et al.* (2015) FtsZ filament capping by MciZ, a developmental regulator of bacterial division. *Proc Natl Acad Sci U S A* **112**: E2130-2138. DOI: 10.1073/pnas.1414242112.

Bisson-Filho, A.W., Y.P. Hsu, G.R. Squyres, E. Kuru, F. Wu, C. Jukes*, et al.* (2017) Treadmilling by FtsZ filaments drives peptidoglycan synthesis and bacterial cell division. *Science* **355**: 739-743. DOI: 10.1126/science.aak9973.

Buske, P.J., A. Mittal, R.V. Pappu & P.A. Levin (2015) An intrinsically disordered linker plays a critical role in bacterial cell division. *Semin Dev Biol* **37**: 3-10. DOI: 10.1016/j.semcdb.2014.09.017.

Copolovici, D.M., K. Langel, E. Eriste & U. Langel. (2014) Cell-penetrating peptides: design, synthesis, and applications. *ACS Nano* **8**: 1972-1994. DOI: 10.1021/nn4057269.

Cordell, S.C., E.J. Robinson & J. Lowe. (2003) Crystal structure of the SOS cell division inhibitor SulA and in complex with FtsZ. *Proc Natl Acad Sci U S A* **100**: 7889-7894. DOI: 10.1073/pnas.1330742100.

de Hoon, M.J.L., P. Eichenberger & D. Vitkup. (2010) Hierarchical Evolution of the Bacterial Sporulation Network. *Current Biology* **20**: R735-R745. DOI: https://doi.org/10.1016/j.cub.2010.06.031.

de la Torre, B.G., V. Hornillos, J.R. Luque-Ortega, M.A. Abengozar, F. Amat-Guerri, A.U. Acuna*, et al.* (2014) A BODIPY-embedding miltefosine analog linked to cell-penetrating Tat(48-60) peptide favors intracellular delivery and visualization of the antiparasitic drug. *Amino Acids* **46**: 1047-1058. DOI: 10.1007/s00726-013-1661-3.

den Blaauwen, T., J.M. Andreu & O. Monasterio. (2014) Bacterial cell division proteins as antibiotic targets. *Bioorg Chem* **55**: 27-38. DOI: 10.1016/j.bioorg.2014.03.007.

den Blaauwen, T., L.W. Hamoen & P.A. Levin. (2017) The divisome at 25: the road ahead. *Curr Opin Microbiol* **36**: 85-94. DOI: 10.1016/j.mib.2017.01.007.

Dereeper, A., V. Guignon, G. Blanc, S. Audic, S. Buffet, F. Chevenet*, et al.* (2008) Phylogeny.fr: robust phylogenetic analysis for the non-specialist. *Nucleic Acids Res* **36**: W465-469. DOI: 10.1093/nar/gkn180.

Du, S. & J. Lutkenhaus. (2017) Assembly and activation of the Escherichia coli divisome. *Mol Microbiol* **105**: 177-187. DOI: 10.1111/mmi.13696.

Egan, A.J., R.M. Cleverley, K. Peters, R.J. Lewis & W. Vollmer. (2017) Regulation of bacterial cell wall growth. *FEBS J* **284**: 851-867. DOI: 10.1111/febs.13959.

Elsen, N.L., J. Lu, G. Parthasarathy, J.C. Reid, S. Sharma, S.M. Soisson*, et al.* (2012) Mechanism of action of the cell-division inhibitor PC190723: modulation of FtsZ assembly cooperativity. *J Am Chem Soc* **134**: 12342-12345. DOI: 10.1021/ja303564a.

Errington, J. (2003) Regulation of endospore formation in Bacillus subtilis. *Nat Rev Microbiol* **1**: 117-126. DOI: 10.1038/nrmicro750.

Freyer, M.W. & E.A. Lewis, (2008) Isothermal Titration Calorimetry: Experimental Design, Data Analysis, and Probing Macromolecule/Ligand Binding and Kinetic Interactions. In: Methods in Cell Biology*. Academic Press* **84**:79-113. DOI: 10.1016/S0091-679X(07)84004-0.

Fujita, J., Y. Maeda, E. Mizohata, T. Inoue, M. Kaul, A.K. Parhi*, et al.* (2017) Structural Flexibility of an Inhibitor Overcomes Drug Resistance Mutations in Staphylococcus aureus FtsZ. *ACS Chem Biol* **12**: 1947-1955. DOI: 10.1021/acschembio.7b00323.

Haeusser, D.P. & W. Margolin. (2016) Splitsville: structural and functional insights into the dynamic bacterial Z ring. *Nat Rev Microbiol* **14**: 305-319. DOI: 10.1038/nrmicro.2016.26.

Handler, A.A., J.E. Lim & R. Losick. (2008) Peptide inhibitor of cytokinesis during sporulation in Bacillus subtilis. *Mol Microbiol* **68**: 588-599. DOI: 10.1111/j.1365-2958.2008.06173.x.

Haraldsen, J.D. & A.L. Sonenshein. (2003) Efficient sporulation in Clostridium difficile requires disruption of the sigmaK gene. *Mol Microbiol* **48**: 811-821. DOI: 10.1046/j.1365-2958.2003.03471.x.

Haydon, D.J., N.R. Stokes, R. Ure, G. Galbraith, J.M. Bennett, D.R. Brown*, et al.* (2008) An inhibitor of FtsZ with potent and selective anti-staphylococcal activity. *Science* **321**: 1673-1675. DOI: 10.1126/science.1159961.

Higgins, D. & J. Dworkin. (2012) Recent progress in Bacillus subtilis sporulation. *FEMS Microbiology Reviews* **36**: 131-148. DOI: 10.1111/j.1574-6976.2011.00310.x.

Huecas, S., E. Ramirez-Aportela, A. Vergonos, R. Nunez-Ramirez, O. Llorca, J.F. Diaz*, et al.* (2017) Self-Organization of FtsZ Polymers in Solution Reveals Spacer Role of the Disordered C-Terminal Tail. *Biophys J* **113**: 1831-1844. DOI: 10.1016/j.bpj.2017.08.046.

Kaul, M., L. Mark, A.K. Parhi, E.J. LaVoie & D.S. Pilch. (2016) Combining the FtsZ-Targeting Prodrug TXA709 and the Cephalosporin Cefdinir Confers Synergy and Reduces the Frequency of Resistance in Methicillin-Resistant Staphylococcus aureus. *Antimicrob Agents Chemother* **60**: 4290-6. DOI: 10.1128/AAC.00613-16.

Kim, S.J., J. Chang & M. Singh. (2015) Peptidoglycan architecture of Gram-positive bacteria by solid-state NMR. *Biochim Biophys Acta* **1848**: 350-362. DOI: 10.1016/j.bbamem.2014.05.031.

Levin, P.A. & R. Losick. (1996) Transcription factor Spo0A switches the localization of the cell division protein FtsZ from a medial to a bipolar pattern in Bacillus subtilis. *Genes Dev* **10**: 478-488. DOI: 10.1101/gad.10.4.478.

Lock, R.L. & E.J. Harry. (2008) Cell-division inhibitors: new insights for future antibiotics. *Nat Rev Drug Discov* **7**: 324-338. DOI: 10.1038/nrd2510.

Malanovic, N. & K. Lohner. (2016) Gram-positive bacterial cell envelopes: The impact on the activity of antimicrobial peptides. *Biochim Biophys Acta* **1858**: 936-946. DOI: 10.1016/j.bbamem.2015.11.004.

Matsui, T., J. Yamane, N. Mogi, H. Yamaguchi, H. Takemoto, M. Yao*, et al.* (2012) Structural reorganization of the bacterial cell-division protein FtsZ from Staphylococcus aureus. *Acta Crystallogr D Biol Crystallogr* **68**: 1175-1188. DOI: 10.1107/S0907444912022640.

Monahan, L.G. & E.J. Harry (2016) You are what you eat: metabolic control of bacterial division. *Trends Microbiol.* **24**: 181-189. DOI: 10.1016/j.tim.2015.11.007

Monteiro, J.M., A.R. Pereira, N.T. Reichmann, B.M. Saraiva, P.B. Fernandes, H. Veiga*, et al.* (2018) Peptidoglycan synthesis drives an FtsZ-treadmilling-independent step of cytokinesis. *Nature* **554**: 528-532. DOI: 10.1038/nature25506.

Nogales, E., K.H. Downing, L.A. Amos & J. Lowe. (1998) Tubulin and FtsZ form a distinct family of GTPases. *Nat Struct Biol* **5**: 451-458. DOI: 10.1038/nsb0698-451.

Pandey, R., A. Ter Beek, N.O. Vischer, J.P. Smelt, S. Brul & E.M. Manders. (2013) Live cell imaging of germination and outgrowth of individual bacillus subtilis spores; the effect of heat stress quantitatively analyzed with SporeTracker. *PLoS One* **8**: e58972. DOI: 10.1371/journal.pone.0058972.

Paredes-Sabja, D., P. Setlow & M.R. Sarker. (2011) Germination of spores of Bacillales and Clostridiales species: mechanisms and proteins involved. *Trends Microbiol* **19**: 85-94. DOI: 10.1016/j.tim.2010.10.004.

Paredes-Sabja, D., A. Shen & J.A. Sorg. (2014) Clostridium difficile spore biology: sporulation, germination, and spore structural proteins. *Trends Microbiol* **22**: 406-416. DOI: 10.1016/j.tim.2014.04.003.

Piggot, P.J. & D.W. Hilbert. (2004) Sporulation of Bacillus subtilis. *Curr Opin Microbiol* **7**: 579-586. DOI: 10.1016/j.mib.2004.10.001.

Pinho, M.G. & J. Errington. (2003) Dispersed mode of Staphylococcus aureus cell wall synthesis in the absence of the division machinery. *Mol Microbiol* **50**: 871-881. DOI: 10.1046/j.1365-2958.2003.03719.x

Ruiz-Avila, L.B., S. Huecas, M. Artola, A. Vergonos, E. Ramirez-Aportela, E. Cercenado*, et al.* (2013) Synthetic inhibitors of bacterial cell division targeting the GTP-binding site of FtsZ. *ACS Chem Biol* **8**: 2072-2083. DOI: 10.1021/cb400208z.

Schaffner-Barbero, C., M. Martin-Fontecha, P. Chacon & J.M. Andreu. (2012) Targeting the assembly of bacterial cell division protein FtsZ with small molecules. *ACS Chem Biol* **7**: 269-277. DOI: 10.1021/cb2003626.

662 Schuck, P., M.A. Perugini, N.R. Gonzales, G.J. Howlett & D. Schubert. (2002) Size-distribution
663 analysis of proteins by analytical ultracentrifugation: strategies and application to model
664 systems. *Biophys J* **82**: 1096-1111. DOI: 10.1016/S0006-3495(02)75469-6.

665 Seydlova, G. & J. Svobodova. (2012) Rapid and effective method for the separation of Bacillus
666 subtilis vegetative cells and spores. *Folia Microbiol (Praha)* **57**: 455-457. DOI: 10.1007/s12223-
667 012-0157-y.

668 Steiner, E., A.E. Dago, D.I. Young, J.T. Heap, N.P. Minton, J.A. Hoch*, et al.* (2011) Multiple
669 orphan histidine kinases interact directly with Spo0A to control the initiation of endospore
670 formation in Clostridium acetobutylicum. *Mol Microbiol* **80**: 641-654. DOI: 10.1111/j.1365-
671 2958.2011.07608.x.

672 Sterlini, J.M. & J. Mandelstam. (1969) Commitment to sporulation in Bacillus subtilis and its
673 relationship to development of actinomycin resistance. *Biochem J* **113**: 29-37.

674 Stokes, N.R., N. Baker, J.M. Bennett, J. Berry, I. Collins, L.G. Czaplewski*, et al.* (2013) An
675 improved small-molecule inhibitor of FtsZ with superior in vitro potency, drug-like properties,
676 and in vivo efficacy. *Antimicrob Agents Chemother* **57**: 317-325. DOI: 10.1128/AAC.01580-12.

677 Sundararajan, K., A. Vecchiarelli, K. Mizuuchi & E.D. Goley. (2018) Species- and C-terminal
678 linker-dependent variations in the dynamic behavior of FtsZ on membranes in vitro. *Mol*
679 *Microbiol*. DOI: 10.1111/mmi.14081.

680 Tan, C.M., A.G. Therien, J. Lu, S.H. Lee, A. Caron, C.J. Gill*, et al.* (2012) Restoring methicillin-
681 resistant Staphylococcus aureus susceptibility to beta-lactam antibiotics. *Sci Transl Med* **4**:
682 126ra135. DOI: 10.1126/scitranslmed.3003592.

683 Wagstaff, J.M., M. Tsim, M.A. Oliva, A. Garcia-Sanchez, D. Kureisaite-Ciziene, J.M. Andreu*, et*
684 *al.* (2017) A Polymerization-Associated Structural Switch in FtsZ That Enables Treadmilling of
685 Model Filaments. *MBio* **8**. DOI: 10.1128/mBio.00254-17.

686 Wang, H.Y. & R.F. Wang. (2012) Enhancing cancer immunotherapy by intracellular delivery of
687 cell-penetrating peptides and stimulation of pattern-recognition receptor signaling. *Adv*
688 *Immunol* **114**: 151-176. DOI: 10.1016/B978-0-12-396548-6.00006-8.

689 Weart, R.B., A.H. Lee, A.C. Chien, D.P. Haeusser, N.S. Hill & P.A. Levin. (2007) A metabolic
690 sensor governing cell size in bacteria. *Cell* **130**: 335-347. DOI: 10.1016/j.cell.2007.05.043.

691 Xiao, J. & E.D. Goley. (2016) Redefining the roles of the FtsZ-ring in bacterial cytokinesis. *Curr*
692 *Opin Microbiol* **34**: 90-96. DOI: 10.1016/j.mib.2016.08.008.

693 Yang, X., Z. Lyu, A. Miguel, R. McQuillen, K.C. Huang & J. Xiao. (2017) GTPase activity-coupled
694 treadmilling of the bacterial tubulin FtsZ organizes septal cell wall synthesis. *Science* **355**: 744-
695 747. DOI: 10.1126/science.aak9995.

696

697

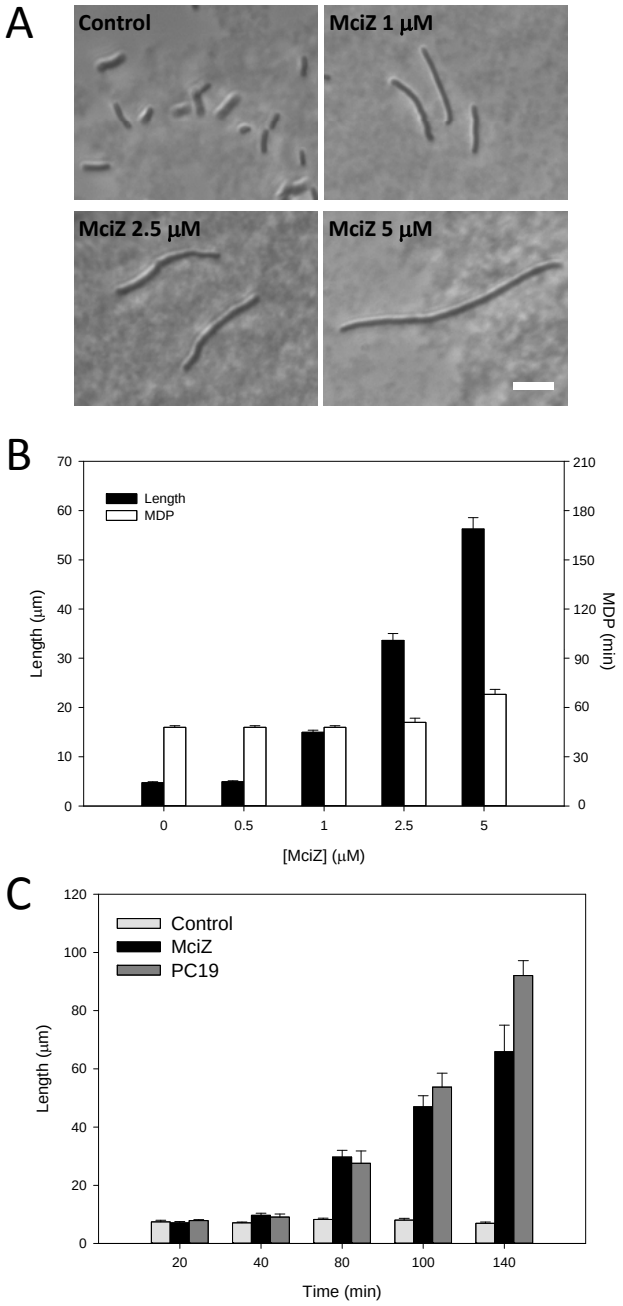

Figure 1. Synthetic peptide MciZ effectively inhibits *B. subtilis* cell division. A. Representative examples of undivided *B. subtilis* 168 cells incubated with different MciZ concentrations during 1.5h (phase contrast; scale bar: 10 μm). **B**. Cell length measurements and mass doubling periods (MDP). The histogram shows the average and standard error from three independent experiments. **C**. Time-course of the effect of MciZ (5 μM) on cell length compared with the small molecule cell division inhibitor PC190723 (5 μM).

A

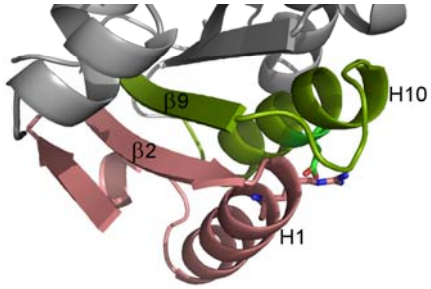

B

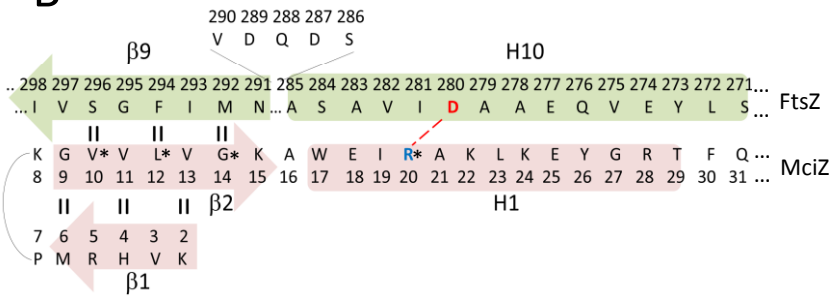

C

Sequence	Amino acid change	Name
MKVHRMPKGVVLVGKAWEIRAKLKEYGRTFQYVKDWISKP	-	MciZ
MKVHRMPKGVVLVGKAWEI**A**AKLKEYGRTFQYVKDWISKP	Arg20 → Ala	R20A
MKVHRMPKGVVLVGKAWEI**D**AKLKEYGRTFQYVKDWISKP	Arg20 → Asp	R20D
MKVHRMPKGVV**P**VGKAWEIRAKLKEYGRTFQYVKDWISKP	Leu12 → Pro	L12P
MKVHRMPKGVV**l**VGKAWEIRAKLKEYGRTFQYVKDWISKP	Leu12 → *D*-Leu	L12l
MKVHRMPKG**V**VLVGKAWEIRAKLKEYGRTFQYVKDWISKP	Val10 → N-methyl-Val	V10^{m}V
MKVHRMPKGVVLV**G**KAWEIRAKLKEYGRTFQYVKDWISKP	Gly14 → N-methyl-Gly	G14^{m}G
MKVYILPNRVTLVGKAWQIRHKLKQYGKEYTTVQEWITASKK	marked in red	MciZ$_{Bant}$

D

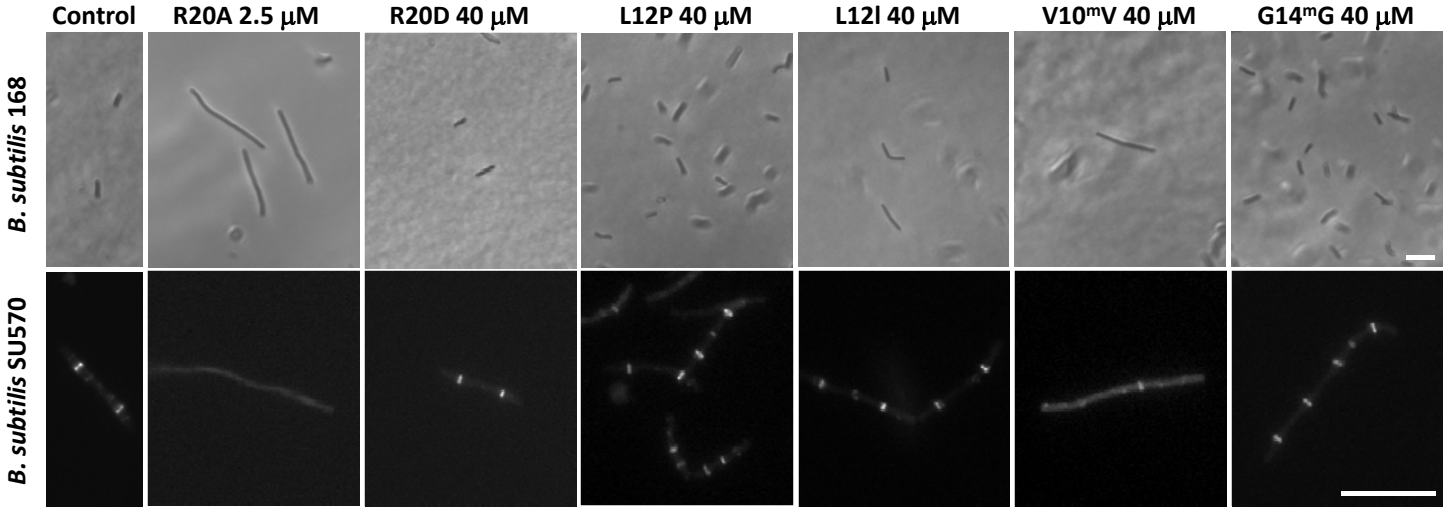

Figure 2. Synthetic MciZ analogs and their effects on *B. subtilis* cell division and FtsZ subcellular localization. A. Structure of MciZ (pale red ribbon diagram) in complex with FtsZ (interacting elements in green) (from PDB entry 4U39 molecule A). MciZ β-strands 1 and 2 extend the C-terminal β-sheet of FtsZ. MciZ helix 1 interacts with FtsZ helix 10; residues Arg20 (MciZ) and Asp280 (FtsZ) (in sticks representation) form a salt bridge. **B.** Schematic representation of the ionic interactions between MciZ and FtsZ, including the hydrogen bonds formed between MciZ strand β2 and FtsZ strand β9. MciZ residues that have been synthetically replaced are marked by asterisks. **C**. Peptide sequences of synthetic MciZ analogs employed in this work. **D**. *B. subtilis* 168 (phase contrast) or *B. subtilis* SU570 (FtsZ-GFP fluorescence) were incubated with MciZ analogs at the concentrations indicated during 1.5 h and their effects on cell length and FtsZ sub-cellular localization were analyzed. Representative images of each observed phenotype are shown (scale bars: 10 μm).

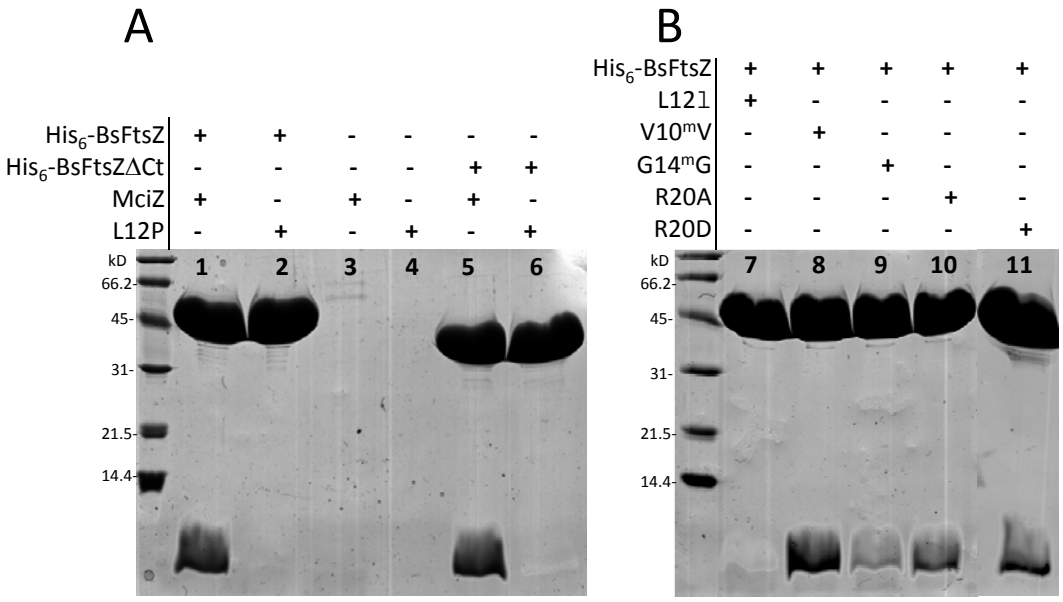

Figure 3. **His-tag pull down assay for FtsZ/MciZ interaction**. **A.** Synthetic MciZ peptides (30 μM) were incubated with purified His_6-BsFtsZ (30 μM) bound trough the N-terminal His-tag to a Ni^{2+} chelating resin. After elution, proteins were subjected to a SDS PAGE and stained with coomassie blue dye. Lanes 1 and 2 are assays with MciZ and variant L12P respectively. Lanes 3 and 4 are controls without His_6-BsFtsZ. Lanes 5 and 6 are similar to 1 and 2 but with truncated protein His_6-BsFtsZΔCt. **B**. Lanes 7-11: pull-down tests with the other MciZ variants.

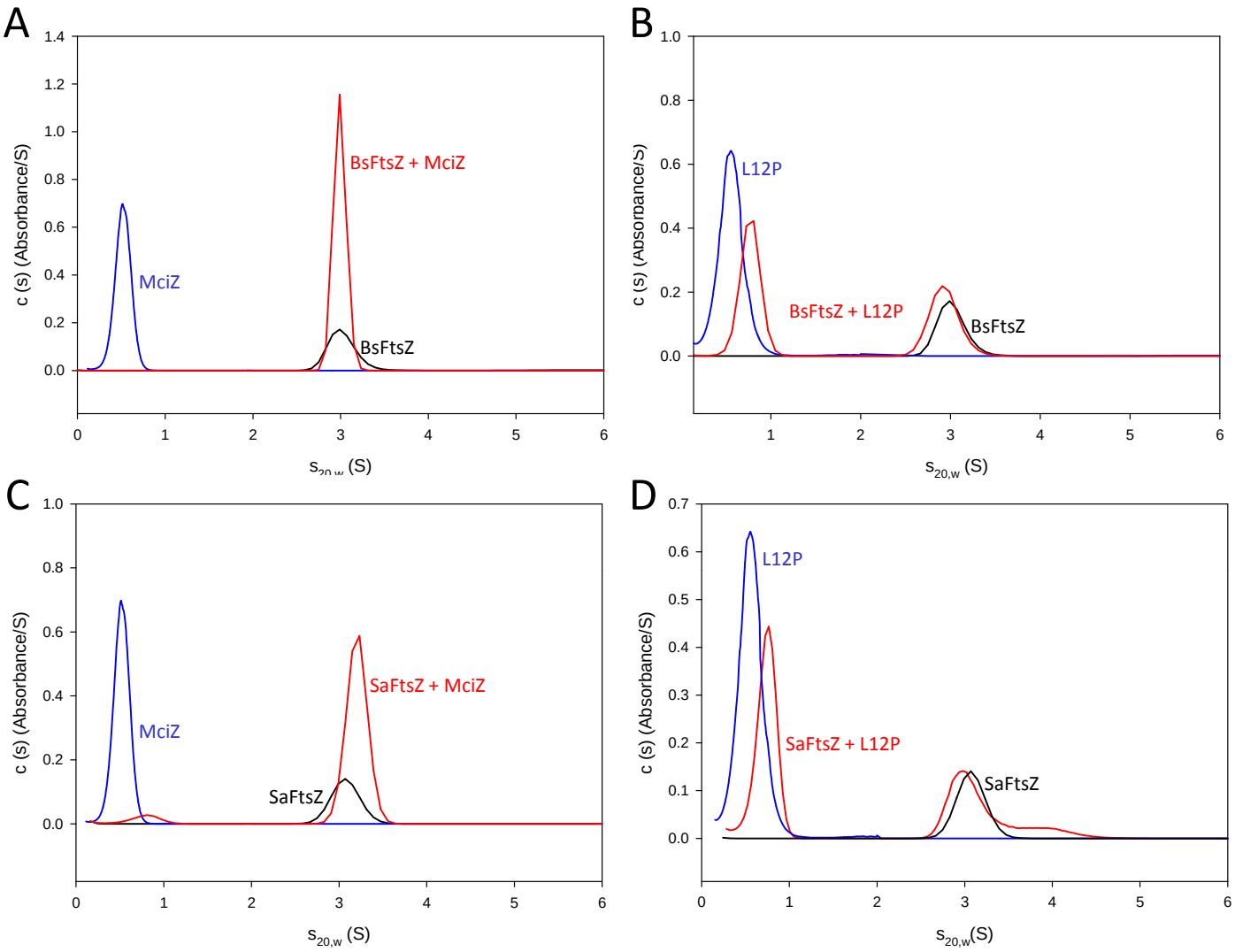

E

Molecules of peptide co-sedimenting per each FtsZ molecule

	MciZ	L12P	R20A	R20D	V10^{m}V	L12I	G14^{m}G
BsFtsZ	0.87	0.16	1.31	0.07	1.00	0.28	1.13
SaFtsZ	0.93	0.01					

Figure 4. Binding of MciZ and L12P to FtsZ analyzed with sedimentation velocity AUC. A-B. Sedimentation coefficient distributions c(s) of 30 μM BsFtsZ (black lines, main peak average $s_{20,w}$= 3.0 S), 30 μM MciZ (A, blue line, 0.5 S), 30 μM L12P (B, blue line, 0.6 S) and the mixtures of 30 μM BsFtsZ with 30 μM MciZ (A, red line, 3.0 S) or with 30 μM L12P (B, red line, 0.8 S and 2.9 S). **C-D.** Sedimentation coefficient distribution c(s) of 30 μM SaFtsZ (black line, 3.1 S), 30 μM MciZ (C, blue line, 0.5 S), 30 μM L12P (D, blue line, 0.6 S) and the mixtures of 30 μM SaFtsZ with 30 μM MciZ (C, red line, 0.8 S and 3.2 S) or with 30 μM L12P (D, red line, 0.7 S and 3.0 S). Absorbance data at 295 nm were acquired to monitor peptide and protein sedimentation. **E.** The concentrations of sedimenting peptide and FtsZ were calculated to estimate binding stoichiometry (Methods; see figure S2 for additional sedimentation coefficient distributions).

A

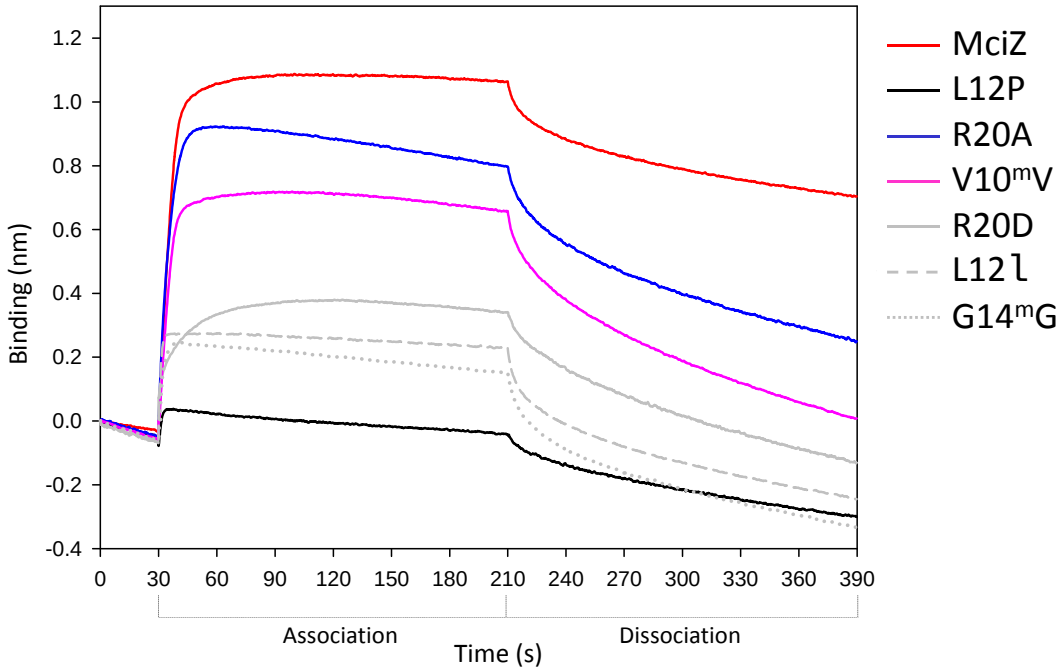

B

Ligand	Analyte	k+ ($M^{-1}\cdot s^{-1}$)	k- (s^{-1})	K_D (μM)
FtsZ	MciZ	$(6.6 \pm 0.5)\cdot 10^{4}$	$(8.8 \pm 4.4)\cdot 10^{-3}$	0.13 ± 0.07
	L12P	-	-	No binding
	R20A	$(9.7 \pm 1.8)\cdot 10^{4}$	$(7.7 \pm 4.0)\cdot 10^{-3}$	0.08 ± 0.03
	V10mV	$(7.7 \pm 2.7)\cdot 10^{4}$	$(8.1 \pm 2.3)\cdot 10^{-3}$	0.11 ± 0.07

Figure 5. Interactions of synthetic MciZ peptides with BsFtsZ. A. Sensorgrams from bio-layer interferometry (BLI) experiments. BsFtsZ (ligand) was immobilized to the tip of the sensor through an His-tag and 2 μM of MciZ or its variants (analytes) were tested for interaction. **B**. Kinetic parameters for the interaction of BsFtsZ with synthetic MciZ analogs. The binding of MciZ to FtsZ was analyzed at different concentrations of peptide and the association rate constant (k+) was determined from the slope of the linear regression line. The dissociation rate constant (k-) and the equilibrium constant values (K_D; calculated for a simple binding model) are the average of four independent experiments with MciZ. Two independent experiments were run for the analogs at 2 μM concentration ($R^2 > 0.97$ in all cases). L12P is an inactive peptide. The interactions of R20D, L12l and G14mG did not adjust to a binding model.

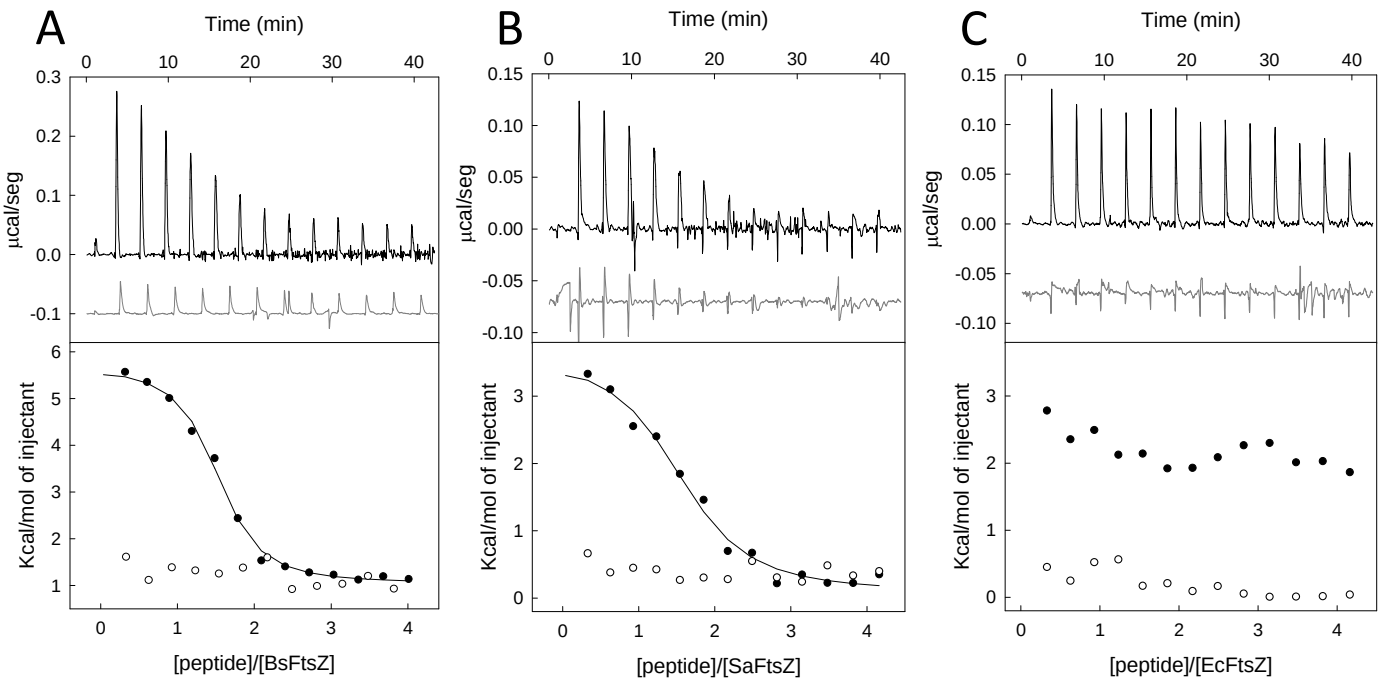

Figure 6. **Calorimetric titrations (ITC)** of MciZ interaction with BsFtsZ (**A**), SaFtsZ (**B**) and EcFtsZ (**C**). MciZ, black line and solid circles; L12P, gray line and empty circles. Each peak (*upper panels*) represents the heat (integrated area) resulting from peptide injection into FtsZ solution. Each point in the *bottom panels* is the heat evolved per mol of injected ligand in the corresponding peak in the *upper panel*, s*olid lines* are the best fits to experimental data. Note that L12P injections in the upper panels are downshifted on the y- axis to facilitate comparison.

Table 1. Energetics of the interactions of MciZ peptides with FtsZ determined by ITC at 25 ^{o}C [a]

Peptide ligand and protein	K_D (µM)	ΔG (kcal mol^{-1})	ΔH (kcal mol^{-1})	-TΔS (kcal mol^{-1})	n
MciZ (BsFtsZ)	0.26 ± 0.15	-8.88 ± 0.18	3.35 ± 0.35	-12.25 ± 0.02	1.5 ± 0.2
MciZ (SaFtsZ)	1.42 ± 0.60	-7.98 ± 0.26	3.53 ± 0.35	-11.51 ± 0.02	1.5 ± 0.2
R20A (BsFtsZ)	0.16 ± 0.10	-9.34 ± 0.06	4.06 ± 0.30	-13.42 ± 0.30	1.5 ± 0.1
L12l(BsFtsZ)	10.8 ± 8.0	-6.79 ± 0.15	6.36 ± 2.80	-13.09 ± 0.30	1.3[b]
V10^{m}V(BsFtsZ)	0.18 ± 0.08	-9.23 ± 0.03	4.71 ± 0.23	-13.95 ± 0.15	1.3 ± 0.1
G14^{m}G(BsFtsZ)	1.85 ± 0.62	-7.21 ± 0.15	7.07 ± 0.50	-14.28 ± 0.06	0.9 ± 0.1

[a] Values are average and standard error of at least duplicate experiments. Values for MciZ(BsFtsZ) are an average of five experiments.
[b] Stoichiometry was constrained to n = 1.3 in this case.

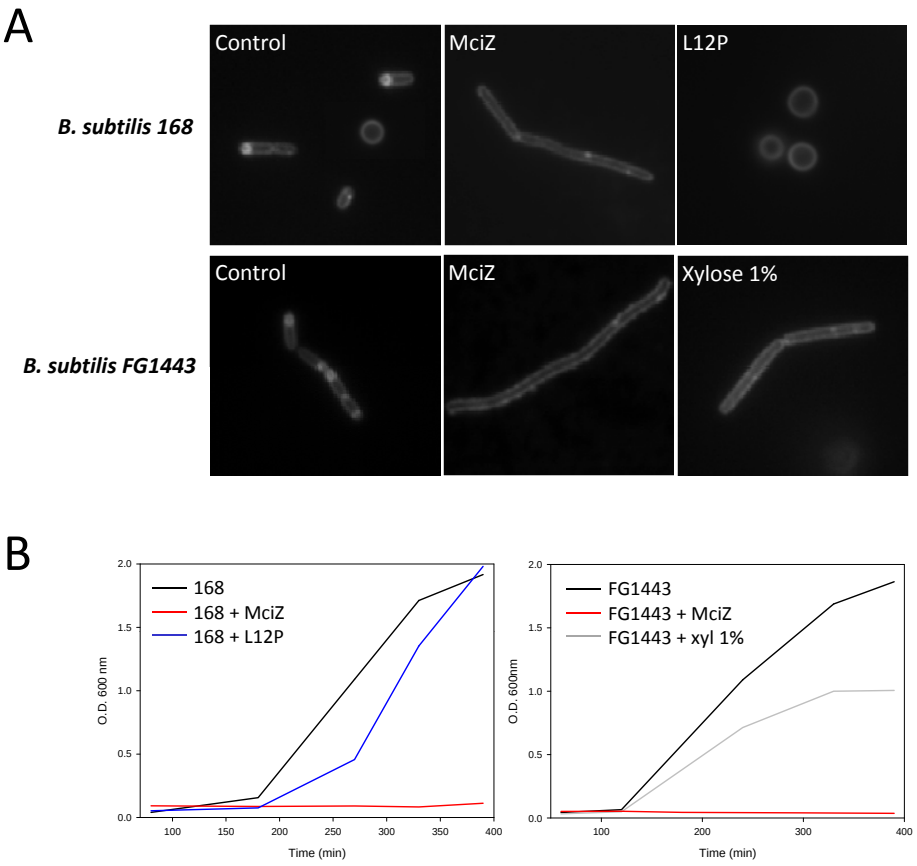

Figure 7. Effects of exogenous and endogenous MciZ on sporulation and germination. A. *B. subtilis* cells were stained with the membrane dye FM4-64 and examined by fluorescence microscopy, 5 h after inducing sporulation. *B. subtilis* 168 was grown in sporulation medium without (control) or with 5 μM MciZ or 5 μM L12P inactive analog, as indicated. *B. subtilis* strain FG1443 (*amyE::Pxyl-mciZ*) -which harbours a xylose-inducible copy of *mciZ*- was grown in sporulation medium without (control) or with 5 μM MciZ or 1 % xylose. **B**. Left: germination curves of *B. subtilis* 168 in the absence or presence of MciZ or L12P (5 μM) added to the culture medium. Right: Germination curves of *B. subtilis* FG1443 in the absence or presence of MciZ (5 μM) or xylose (1%).

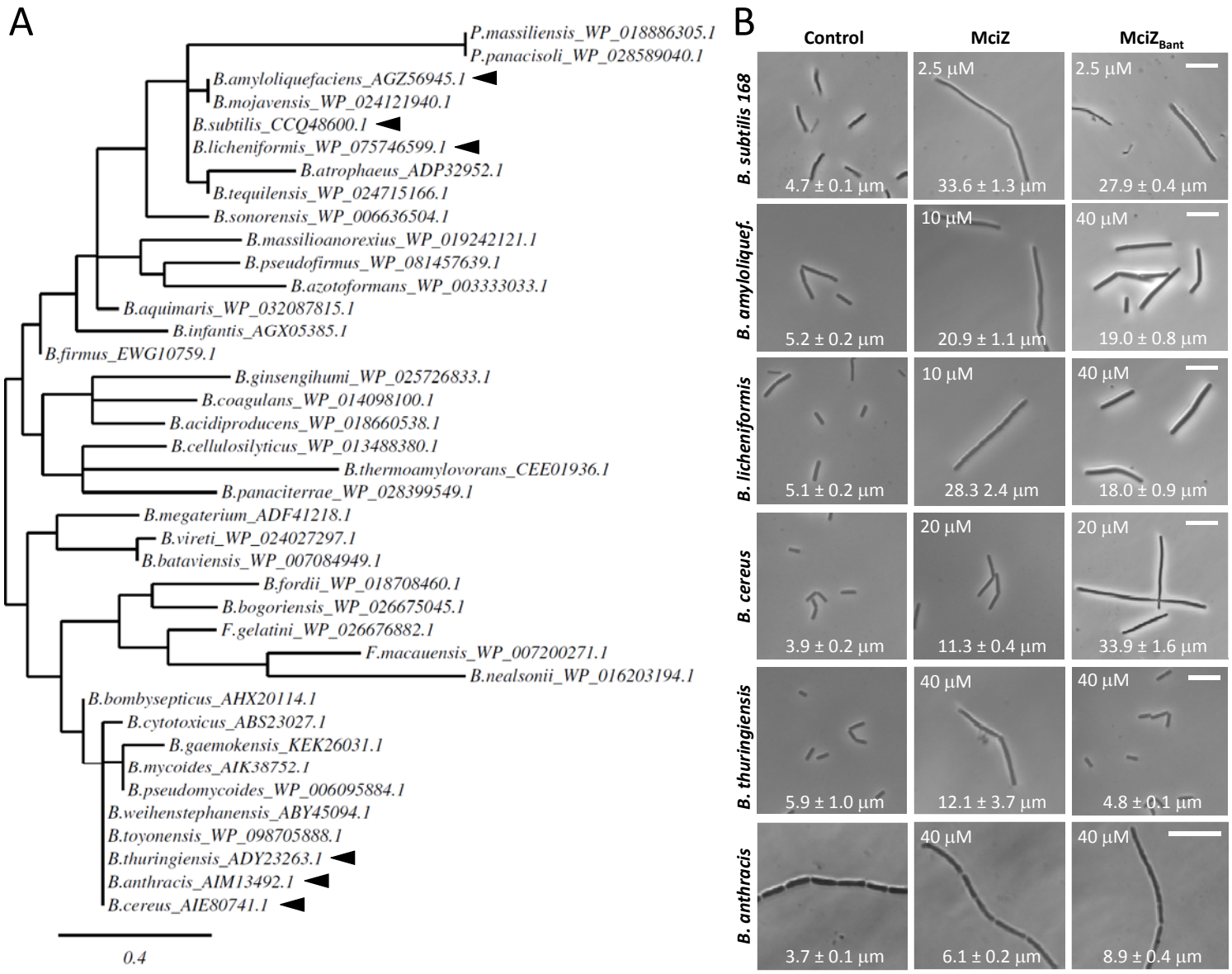

Figure 8. Effect of synthetic *B. subtilis* and *B. anthracis* MciZ on phylogenetically related *Bacillus* species. A. Phylogenetic tree of *Bacillus* species based on MciZ protein sequences. Sequences were obtained from GenBank and NCBI. Accession numbers for each sequence are shown. Branch length is proportional to estimated phylogenetic distance, in amino acid substitutions per site. Arrowheads: *Bacillus* species selected for *in vivo* studies. **B.** Cells of *Bacillus spp.* were incubated during 3 h with MciZ or $MciZ_{Bant}$ and their effects on cell length were analyzed under the microscope using phase contrast. Representative examples of each observed phenotype are shown (scale bars: 10 µm). The peptide concentrations employed and mean cell lengths are indicated in each case.

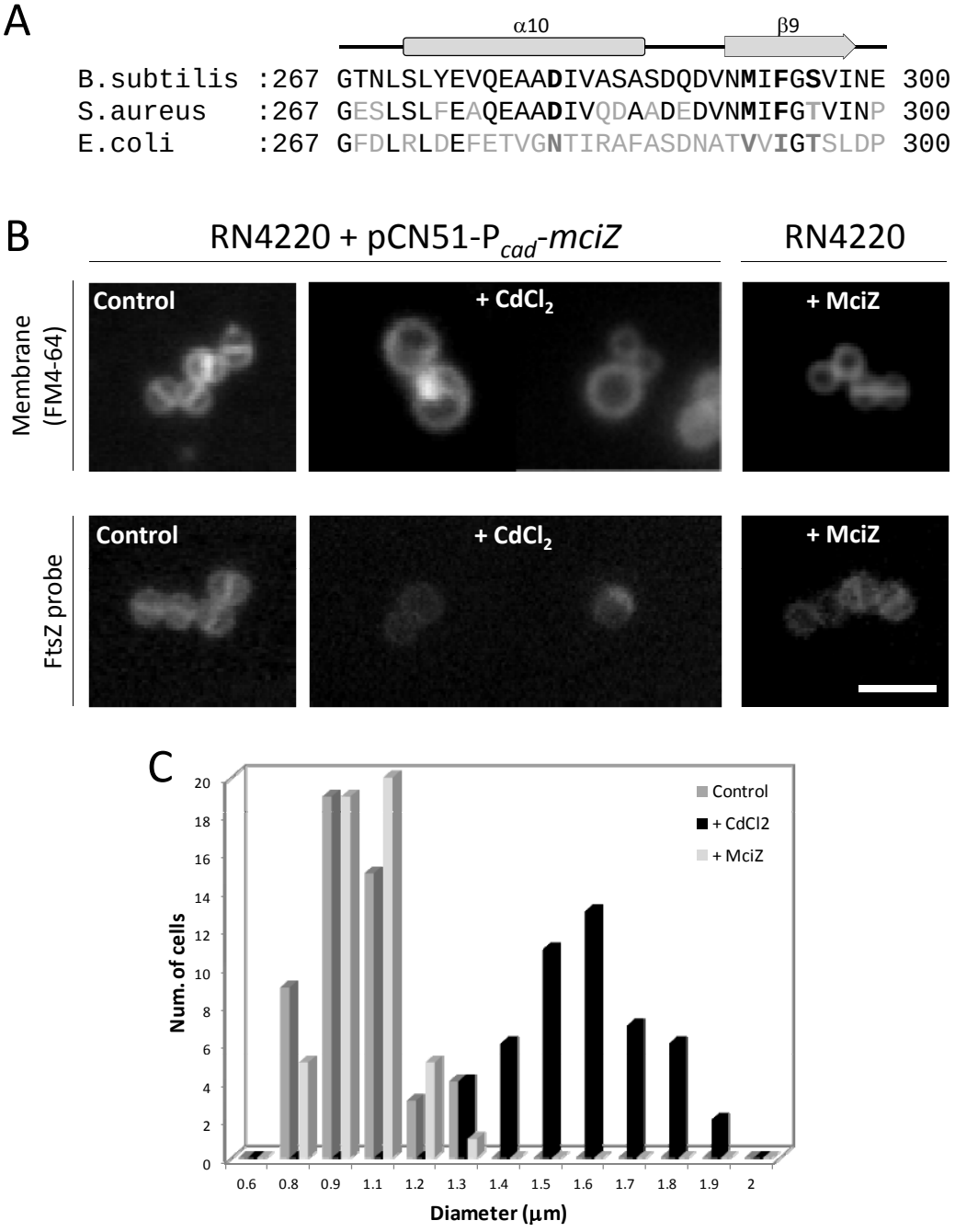

Figure 9. Effects of MciZ on cell division in *S. aureus*. **A**. Protein sequence alignment for FtsZ from *B. subtilis*, *S. aureus* and *E. coli*. In bold are shown residues involved in ionic interactions with MciZ. **B**. *S. aureus* RN4220 cells harboring a plasmid with a cadmium-inducible copy of *mciZ* (RN4220 + pCN51-P_{cad}-*mciZ*) were grown in TSB at 37ºC for 5 hours in the absence (Control) or presence of 2.5 µM $CdCl_2$. Cell membranes were stained with FM4-64 and FtsZ was visualized using a fluorescent probe. No effect was observed in RN4220 cells growing in the presence of 40 µM synthetic MciZ (right panel). Scale bars: 2.5 µm. **C**. Diameter measurements of cells from the experiment shown in panel B (n = 50). Control and RN4224+MciZ *S. aureus* cells were 1.00 ± 0.01 µm in diameter. *S. aureus* cells treated with $CdCl_2$ were 1.55 ± 0.02 µm in diameter.